PreFlap: From Photoacoustic Tomography Images to Vascular Mapping Sheets for Improved Preoperative Flap Evaluation

Maria Chiara Munisso, Chang Liu, Goshiro Yamamoto, Tomoko Kosaka, Itaru Tsuge, Susumu Saito, Naoki Morimoto

***Abstract*— Advancements in technology have improved image acquisition and processing in the field of medical imaging, giving medical doctors the tools to implement effective medical care. In plastic surgery, despite advances in anatomical knowledge and technology, problems in preoperative planning for flap surgery remain. In this study, we propose a new protocol to analyze three-dimensional (3D) photoacoustic tomography images and generate two-dimensional (2D) mapping sheets that can help surgeons identify perforators and the perfusion territory during preoperative planning. The core of this protocol is PreFlap, a new algorithm that converts 3D photoacoustic tomography images into 2D vascular mapping images. Experimental results demonstrate that PreFlap can improve preoperative flap evaluation, thus can greatly saving surgeons' time and improving surgical outcomes.**

***Index Terms*— Photoacoustic tomography, Preoperative evaluation, Flaps, Perforators, Perfusion territory**

I. Introduction

RECONSTRUCTIVE plastic surgery can restore the functionality and normal appearance of body parts. However, reconstruction of soft tissue defects, especially those involving exposure of deep vital structures, still remains challenging.

The introduction of perforator flaps, the development of new technologies, and deeper knowledge of vascular anatomy have permitted the dissection of thinner flaps, which are currently expanding opportunities in reconstructive surgery [1], [2]. The concept of perforator flaps is based on a vessel perforating the deep fascia. This large vessel gives off smaller branches that run superficially to supply the overlying skin and subcutaneous tissue. Perforators, which are artery-vein bundles, can be dissected through the muscle to their origin, allowing for the preservation of the functionality of the underlying muscle. Thus, perforator flaps have become a method of choice for most surgeons because they can preserve muscle function and enable less invasive and more complex reconstruction, they have become a method of choice for most surgeons [1]–[4].

Preoperative knowledge of perforator anatomy can expedite flap harvesting, prevent complications (e.g., vessel injury while elevating flaps) and reduce the risks of adverse outcomes [5]. Thus, the first major preoperative step is to determine the number, location, and course of the perforators. However, the exact position of the perforators varies significantly between individuals. Thus, preoperative vascular mapping has been introduced [6]–[8]. Several devices, such as Doppler ultrasonography (US), computerized tomographic angiography (CTA), magnetic resonance angiography (MRA), and fluorescent angiography [9]–[11], have been developed to define the vascular architecture of flaps. One of the main advantages of US is real-time assessment [10]. The main disadvantages of this technique are the operator dependence and the lack of anatomical detail. Practically, the investigation should be performed by skilled personnel with knowledge of flap anatomy [11], [12]. Moreover, US does not reproduce a two-dimensional (2D) or three-dimensional (3D) image of the entire vascular architecture. CTA is widely used for perforator mapping because it can provide a 3D representation of a perforator's pattern from its origin. However, a high dose of radiation is required for delicate superficial branch visualization [6], [9]–[11]. Thus, although CTA is a good method for mapping the vascular architecture of flaps, US is the most popular tool for determining suitable perforators in clinical practice [1], [2], [9]–[11]. In the inferior epigastric perforator (DIEP) flap, for example, surgeons mainly use the support of specific structures such as coordinates relative to the umbilicus, which have been investigated in many cadaveric studies [13]–[15], to identify the area most likely to yield perforators suitable for surgery. With US analysis, surgeons can predict the location where a perforator exits the fascia but cannot accurately determine its subcutaneous course. The most probable location of the perforators is marked on the skin with a pen based on surgeon experience. Therefore, careful dissection is needed during the flap elevation. Consequently, the procedure requires a long time (Fig. 1(a)). To overcome these disadvantages, the precise location of the perforators and their anatomy should be investigated before surgery using information obtained with volumetric imaging techniques, such as CTA. However, the 3D information can

This research was supported by Japan Agency for Medical Research and Development (AMED) under grant number JP22he2302002, and JSPS KAKENHI Grant Numbers JP22H03632.

M. C. Munisso, T. Kosaka, I. Tsuge, S. Saito, N. Morimoto are with Department of Plastic and Reconstructive Surgery, Graduate School of Medicine, Kyoto University, Japan (e-mail: munisso@kuhp.kyoto-u.ac.jp).

C. Liu and G. Yamamoto are with Department of Medical Informatics, Graduate School of Medicine, Kyoto University, Japan.

This article has been accepted for publication in IEEE Transactions on Biomedical Engineering. This is the author's version which has not been fully edited and content may change prior to final publication. Citation information: DOI 10.1109/TBME.2023.3293812

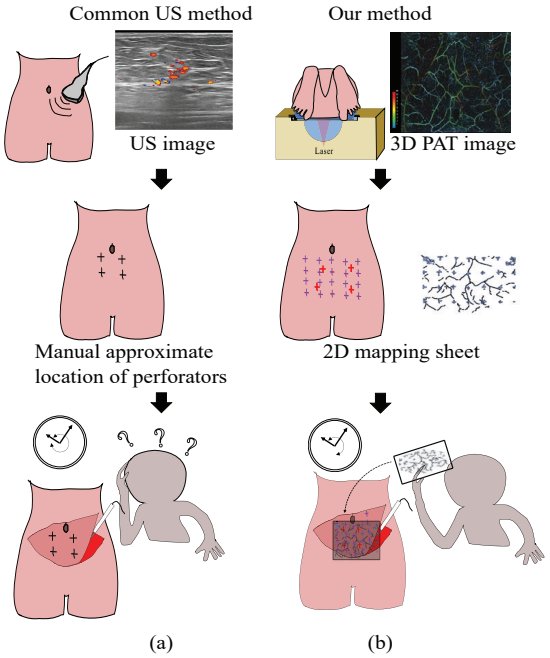

Fig. 1. Pictorial representation of two preoperative and intraoperative flap evaluation methods. (a) Common US preoperative planning method. Surgeons identify the approximate location of the perforators by using US. During the surgery, careful dissection is needed to avoid complications such as vessel injury. Consequently, the procedure requires a long time. (b) Our method. Surgeons are able to identify perforators based on a 2D mapping sheet generated from 3D PAT imaging. The 2D mapping sheet can support the dissection procedure, which can enhance the surgeon's confidence during surgery and reduce operative time.

be difficult to conceptualize intraoperatively. Shen et al [16] used CTA in combination with a printed template to reproduce perforator information on an anterolateral thigh (ALT) flap intraoperatively. The method was more accurate than US, but this film was not curved, so it generated some inaccurate measurements. Indeed, the authors stated that the measurement errors between the CTA results and the actual positions were were larger than 5 mm. Hummelink et al [17] created DIEP flaps by using CTA combined with projection techniques by reproducing the CTA images onto the abdomen during the surgery. They achieved a significant time reduction during the DIEP flap harvesting and accurate identification of more perforators without increasing complications. However, their study only evaluated DIEP flaps. In the prone position, the abdomen area is almost flat; thus, the deformations of projected 3D images due to body curvature were almost absent. In addition, in most of the previously published reports, that used CTA for perforator mapping, information about subcutaneous vessels were not included [6], [9]–[11], [16], [17]. Although projection mapping is interesting, a main problem still remains: surgeons also need information about perforators when the flap is elevated and when it is turned upside down.

Therefore, there has been increasing interest in recent years in developing non-invasive, simple, and accurate methods to represent the vascular architecture of flaps and provide complete 2D and 3D vascular maps that can be used in preoperative planning.

Photoacoustic tomography (PAT) is a new vascular imaging system that uses pulsed laser light to generate ultrasound waves based on the thermoelastic effect. In fact, oxyhemoglobin and deoxyhemoglobin can be used as endogenous contrast substances to provide information on the structure of blood vessel patterns. Thus, PAT is a promising tool for improving preoperative planning for flap surgeries [18]–[21]. In 2018, Tsuge et al [19] showed that PAT and US have comparable diagnostic potential, but PAT was superior in visualizing subcutaneous microvessels. In 2020, Tsuge et al [20] showed that PAT could be used as a diagnostic imaging modality to identify ALT perforators. Moreover, the authors presented a technique to transfer manually the coordinate data of perforators to a body-attachable transparent sheet. The main limitation of that study was the lack of a surgical navigation method to directly apply the vascular images onto the patient. The mapping sheets had to be manually prepared, and they do not provide accurate vascular maps in a timely manner. Moreover, although the morphological appearance of the triple-bundle pattern helps identify perforators, it was not possible to visualize arteries and veins separately for vascular mapping.

Therefore, in this study, we have addressed the main issues reported by Tsuge et al [20] and reached a higher quality of output. Our work mainly focused on the idea that a simple 2D vascular map, obtained from 3D PAT imaging can highlight anatomical variations, assist the surgeon in choosing the appropriate perforator and perfusion territory during preoperative planning, and thus support the dissection procedure. These functions can enhance the surgeon's confidence during surgery and make the procedure faster and more reliable (Fig. 1(b)). The new findings and technical improvements of our study can be summarized as follows:

- Development of an algorithm, denoted as PreFlap, that can "unwrap" 3D PAT images and create 2D mapping sheets that match the body surface automatically without artifact. Thus, the vascular vessels are not drawn by hand from projected images; instead they are interpolated from the 3D data.
- Realization of 2D mapping sheets of artery and vein patterns to localize perforators, branches and perfusion areas. These sheets can be placed on the body surface and help the surgeon to identify vessels, perforators, and perfusion areas intraoperatively. This determines an improvement of the measurement accuracy from about 10 mm [20] to less than 5 mm.
- Design of a clinical trial protocol for ALT and DIEP flaps to improve the overall standard of the previous protocols. Thus, from one type of flap [19], [20] we have expanded the relevance of the clinical protocol to a wider range of flaps.

This study contributes to guideline development for a robust clinical study protocol, which is important for collecting the clinical data needed to elucidate the risk-benefit profile of medical equipment, specifically for the application of PAT in medicine. However, the particular significance of this study lies in the development of PreFlap. In fact, PreFlap reduces

This article has been accepted for publication in IEEE Transactions on Biomedical Engineering. This is the author's version which has not been fully edited and content may change prior to final publication. Citation information: DOI 10.1109/TBME.2023.3293812

measurement errors associated with the localization of vessels and perforators and provides an automated approach to creating 2D maps without concerns about scale and placement on the drawing sheet that accompanies hand drafting in the previous protocol [20].

II. Materials and Methods

A. PAT imaging system

The LUB-0 PAT imaging system is a photoacoustic imaging system developed by Luxonus, Inc. (Kanagawa, Japan) [22]. In brief, the system has ultrasound transducers in a hemispherical arrangement (HDA). The HDA container is filled with water to provide an acoustic coupling medium. In addition, a transparent bag filled with water is positioned on the body surface to allow for smooth transmission of ultrasonic waves to the HDA. When pulsed laser light illuminates the sample, the light-absorbing molecules absorb the light energy, producing localized heating that causes thermoelastic deformation and generates acoustic waves detected by transducers in the HDA.

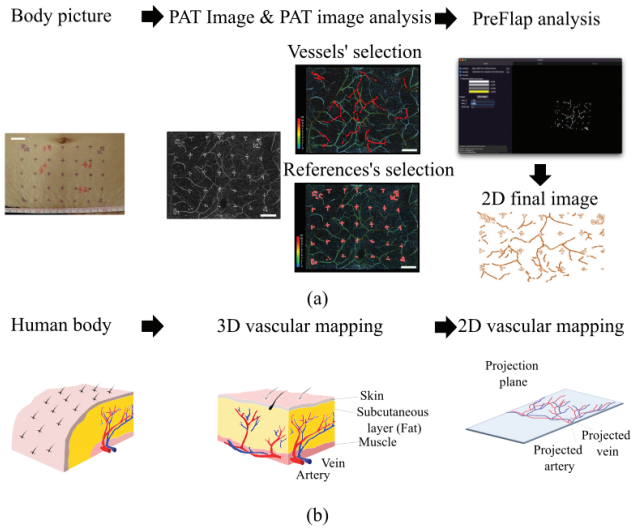

Fig. 2. (a) Pictorial representation of workflows and methods. (b) Schematic flap section with representative blood vessels and planes. White scale bar represents 2 cm.

The reconstructed volumetric image is generated in real time using the universal back projection method [22]–[25]. The LUB-0 system acquires images in two modes: (i) the still scan mode collects large images in few minutes and (ii) the high-resolution mode collects images with an increased number of overlaps that increases the acquisition time but improves the signal-to-noise ratio. The device is equipped with a Ti:sapphire laser. Images can be collected at two wavelengths (797 nm and 756 nm) using either the alternating irradiation mode, in which the two wavelengths oscillate at 15 Hz, or the single wavelength mode, in which only one of the wavelengths is irradiated at 30 Hz.

In this study, all images were collected in the alternating irradiation mode. Each maximum energy of the laser at 756 nm and 797 nm was 8.4 mJ/cm^2 and 10.2 mJ/cm^2, less than the maximum permissible exposure defined by the international standards. PAT images can be displayed in three different display modalities: (i) monochrome 3D image (black and white mode), where vessels are in white and the background is in black; (ii) 3D depth heatmap, where the colors represent the z-depth from the interface between the water bag and the scanning stage with the HDA (depth mode); and (iii) 3D s-factor heatmap, where the colors indicate different s-factor values (s-factor mode). The reconstruction depth is 30mm in depth and the field of view (FOV) of each image is also 30mm. S-factor is an approximate value that is closely correlated with hemoglobin oxygen saturation [23]. It is not possible to visualize the body surface (skin tissue) directly with the LUB-0 system, so an additional software program (PAT viewer) was developed to analyze the images and estimate the body surface using a cloth simulation [26].

B. PreFlap Paradigm

This section outlines the geometric properties of the 3D-to-2D transformation, as well as the paradigm for PreFlap, a graphical user interface (GUI) for converting images from 3D PAT images to 2D mapping images. 3D analysis enables better visualization and it captures details of the vascular architecture. However, it is useful to have a 2D visualization map during surgery to guide surgeons. Thus, taking into consideration the clinical applicability of 2D analysis, we enhanced a standardized image processing workflow to convert 3D PAT images to 2D mapping images as shown in Fig. 2(a). The core of the protocol is a software program that can convert 3D images in 2D projections. The basic idea is that a 3D object projected onto a 2D image plane does not necessarily preserve the object's true shape. Thus, to make meaningful projected 2D images, it is necessary to project the network of the blood vessels onto the skin surface and then rectify the entire visible network on a projection plane as shown in Fig. 2(b). This unwrapping/ rectification produces a final 2D image on which the vessels and perfusion area can be identified to support the planning of flaps in several reconstructive surgeries (Fig. 3(a) and (b)).

1) The unwrapping procedure: Fig. 3(c) is a schematic of the unwrapping procedure. The term unwrap is used to describe the geometric transformation from a randomly shaped body surface to a plane. This section introduces the details of the calculation, which can be broken down into 2 steps: (i) projection from the 3D PAT image perspectively onto the body surface and (ii) projection from the body surface onto the target plane. In the first step, we project points on blood vessels onto the body surface by applying an orthographic projection. The vessels and body surface points are obtained from the PAT viewer as sets of discrete 3D coordinates. However, since the tracked vessel coordinates are achieved as lines of single pixels, the coordinates of the vessels are re-calculated in the 3D rendering. In other words, the number of pixels in the 3D rendering of vessels, which correspond to real physical measurements, is quantified providing an adjustable scaling factor s. Thus, an iterative parameter-fitting algorithm is applied to each pixel obtained by the PAT viewer and its nearby pixels included in a region of space delimited by s.

This article has been accepted for publication in IEEE Transactions on Biomedical Engineering. This is the author's version which has not been fully edited and content may change prior to final publication. Citation information: DOI 10.1109/TBME.2023.3293812

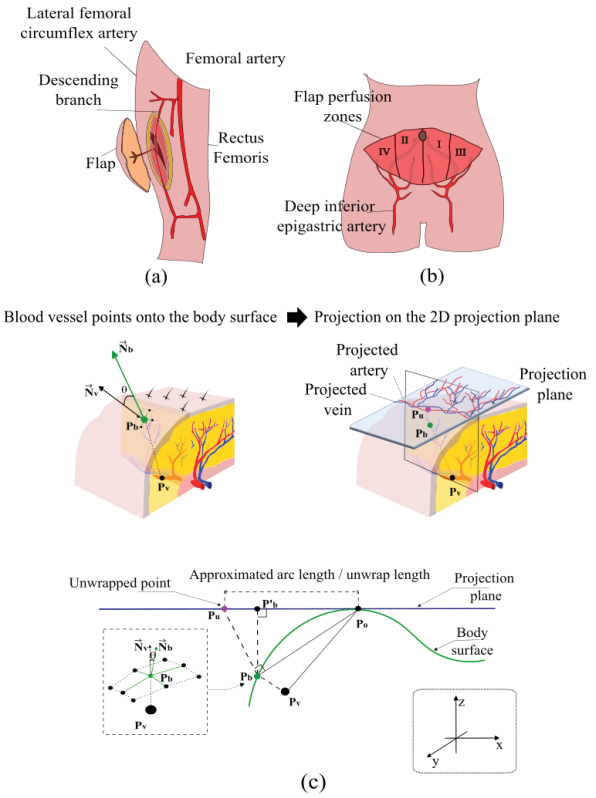

Fig. 3. Schematics of (a) anterolateral thigh and (b) transverse abdominal flaps and (c) the projection system used in PreFlap to convert 3D images into 2D images.

The following results are based on $s = 10$ pixels, which was defined by an experienced surgeon. To explain the algorithm in detail, we first define the parameters shown in Fig. 3(c).

The 3D coordinates corresponding to a point on a blood vessel are represented as the coordinates of a generic point $\mathbf{P_v}$. Generic projected points on the body surface are defined as $\mathbf{P_b}$. For each $\mathbf{P_b}$, we define a normal vector $\mathbf{N_b}$ on the surface based on four nearby points, as well as the directional vector $\mathbf{N_v}$ from $\mathbf{P_v}$ to $\mathbf{P_b}$. With θ defined as the angle between $\mathbf{N_b}$ and $\mathbf{N_v}$, an iterative algorithm is then applied to calculate the target orthographic projection point $\mathbf{P_b}$ where θ is minimized.

In the second step, the point $\mathbf{P_b}$ is projected on the projection plane, which is the plane tangent to the body surface at $\mathbf{P_o}$, approximating the arc from $\mathbf{P_b}$ to $\mathbf{P_o}$. The objective is to compute $\mathbf{P_u}$ from the coordinates of $\mathbf{P_b}$ in 3D space. Because the point $\mathbf{P_u}$ lies on a plane, the z-coordinate has been set to zero. In other words, $\mathbf{P_u}$ is comparable to a 2D point, and it is defined with respect to a 2D coordinate system where $\mathbf{P_o}$ is defined as the center of the 2D space. Thus,an estimation approach using the modulus ratio of the vectors $\mathbf{P_bP_o}$ and $\mathbf{P_vP_o}$ are used to unwrap 3D points on the 2D surface, on which the image of the 3D space will be represented. Thus, to compute $\mathbf{P_u}$ we adjusted the coordinates of the point $\mathbf{P'_b}$, which is the orthographic projection of $\mathbf{P_b}$, with an approximation parameter c, defined as:

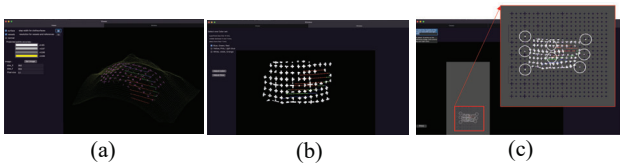

Fig. 4. Labeled image of the 2D image software graphical user interface. (a) 3D view of the vessels, skin, and projected 2D image. In this window, it is possible to change the image parameters. (b) Projected 2D image. It is possible to change the set of colors based on vessel depth in this window. (c) Windows to adjust the image size according to the reference system in order to print a 2D image at the real size.

$$c = \frac{||\overrightarrow{\mathbf{P_bP_o}}||}{||\overrightarrow{\mathbf{P_vP_o}}||}. \tag{1}$$

Thus the $\mathbf{P_u}$ coordinates can be calculated as

$$\begin{bmatrix} \mathbf{P_u(x)} \\ \mathbf{P_u(y)} \\ \mathbf{P_u(z)} \end{bmatrix} = \begin{bmatrix} \mathbf{P_o(x)} + c(\mathbf{P'_b(x)} - \mathbf{P_o(x)}) \\ \mathbf{P_o(y)} + c(\mathbf{P'_b(y)} - \mathbf{P_o(y)}) \\ 0 \end{bmatrix} \tag{2}$$

2) Creation of 2D images (PreFlap Software): Software implementation was performed in XCode (Objective C) for ease of optimization, GUI development, and customization. Fig. 4 depicts the GUI. The images collected with PAT were analyzed with the PAT viewer to create files containing information about: (i) the cloth simulation, which is an approximation of the object surface; (ii) coordinates of references shaped like crosses; and (iii) the coordinates of the tracked vessel. These files were saved by the PAT viewer and then used in PreFlap. In the PAT viewer, the body surface was estimated by the cloth simulation [26]. The file was automatically saved as a binary file. However, to analyze the images, it is important to have some references (violet crosses), which can help with the localization of points that correspond to the images and the human body. The color violet was selected because it is visible in the images collected at 756 nm and barely visible at 797 nm. In the PAT viewer, the user must manually select the references (violet crosses) after selecting the node mode. Next, the user must select and track the blood vessels using the trace mode. PreFlap uses cloth simulation to create the outer interface (object surface) and other files to draw the reference crosses and blood vessels (Fig. 4(a)) in the 3D rendering image. The user can change the step width for the cloth surface, vessels, and crosses in the PreFlap interface (Fig. 4(a)). In this 3D window, it is possible to rotate, translate, and zoom in and out. It is important to check for the correct arrangement of the selected blood vessels and eventually identify anomalies in the 3D vascular architecture. In the 2D window (Fig. 4(b)) it is possible to see the 2D projection. After selecting "Adjust size," the size of the 2D image can be adjusted for printing (Fig. 4(c)). This adjustment is done by selecting eight points in the 2D images and then selecting the corresponding points on the background image to correct printing deformations due to differences in page size.

This article has been accepted for publication in IEEE Transactions on Biomedical Engineering. This is the author's version which has not been fully edited and content may change prior to final publication. Citation information: DOI 10.1109/TBME.2023.3293812

III. Experiments

A. Phantom Experiment

An ideal material that mimics tissue for PAT phantoms would simultaneously possess optical and acoustic properties that are both tunable and biologically relevant. PAT phantoms have been fabricated using many materials, including paraffin gel wax and hydrogels such as gelatin and agarose [27]. Tissue-mimicking phantoms are important for objective and quantitative evaluation of fundamental image characteristics [27]–[30]. In this study, our goal was to develop tunable phantoms to enable the evaluation of simulated small vessels with PAT to validate the ability of PreFlap to convert 3D images in printed 2D maps. To this end, we decided to create phantoms using agarose gel that offers simple and fast preparation.

1) Protocol to create phantoms: Briefly, 5% agarose powder (Agarose S, cat:312-01193, Nippon Gene, Toyama, Japan) in water was heated in a microwave oven until the agarose was completely dissolved. The solution was immediately poured into a silicon mold. Molded phantoms in the shape of semi-cylinders with a diameter of 40 mm and 40 mm thick were created (Fig. 5). To simulate small vessels, 4-0 suture in black nylon (Bear Medic Corporation, Tokyo, Japan) and mechanical pencil leads, (HB 0.5 × 60 mm; UNI, Japan) were used. The sutures were inserted into the mold during the pouring of the gel. The leads were inserted into solid gel (Fig. 6(a)). A total of three imaging phantoms were fabricated: two phantoms were created using the leads (Fig. 5(a) and Fig. 5(b)) and one was created using the suture (Fig. 5(c)). The proposed phantoms and target geometries are compatible with the resolution (0.177 mm), imaging depth ($<$ 30 mm), and field of view (cylinder shape: 30 mm (H) × 22 mm (diameter of circular base)) of the LUB-0 system [22].

2) PAT images: To analyze the images, it is important to estimate the object's surface, i.e., the interface between the phantom and the water bag. This surface is necessary to create a complete 3D-rendered image and then properly adjust the 2D map. However, while the PAT viewer can estimate the body surface easily from clinical images, it is not possible to estimate this surface in the phantoms [26]. Therefore, a film with printed violet crosses was applied to the surface of the phantoms before PAT image acquisition (Figs. 6(b) and (c)). 5 × 5 mm grid pattern of crosses was created using PowerPoint and printed using a ultraviolet printer (VersaUV LeF-12i, Roland DG Co., Hamamatsu, Japan) on Tegaderm (3M, Hudson Rd, Maplewood, MN 55144, USA). The phantom was imaged in regions of approximately 99 mm × 95 mm (Fig. 6(d)). The color violet was selected because it is visible in images collected at 756 nm and barely visible at 797 nm. This allows the user to have two clear images, one to estimate the object surface (at 756 nm) and one to select the leads or blood vessels in the clinical images (at 797 nm).

3) Phantom Experiment Results: Geometric accuracy was estimated based on the overlap between the 2D printed images and the phantoms (Fig. 7). Images were analyzed to evaluate parameters such as arc length, suture and lead length (Fig. 8). The accuracy for the references (violet crosses) was evaluated by measuring the discrepancy between the 2D points obtained from PreFlap and actual distances on the object's surface with a ruler. Images were used to evaluate lead length arc length, to verify that the 2D images were properly unwrapping the images of 3D objects. Table I shows PAT images, 2D images, and images of the overlap between phantoms and 2D images. Tegaderm is a film that becomes opaque over time. Although on the day of the PAT experiments it was possible to see some of the leads in the phantom, it was not possible 1 day later. Therefore, from these images it is possible only to observe a good match between the reference crosses on the phantoms (violet crosses) and 2D-printed images (grey crosses). The error is smaller than 1 mm in these highly curved phantoms (i.e., semicylinders with a radius of 40 mm). The comparison of lead length in the different images confirmed that samples were not deformed by the unwrapping procedure (Table I).

The results of the geometrical analysis of phantom 3 are summarized in Fig. 8. The lengths of arch A, chord C, and sagitta S were evaluated with geometrical calculations and then compared with the data obtained in the 2D images. To assess the accuracy of the 2D mapping function, the most important

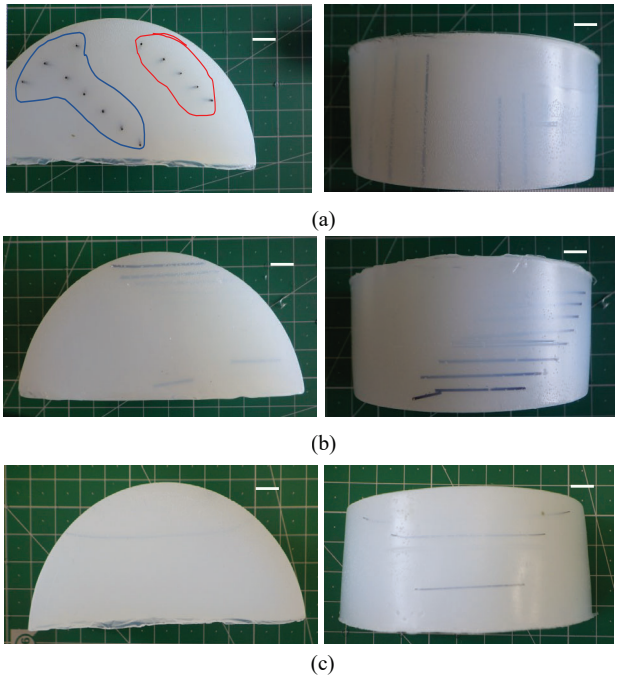

Fig. 5. Top and side views of the phantoms. (a) Phantom 1: the 2 cm leads are in the area outlined in red and the 3 cm leads are in the area outlined in blue. (b) Phantom 2. (c) Phantom 3. White scale bar represents 1 cm.

TABLE I
Lead Length Measurement Results of Phantom 1 and 2

Phantom	Number of leads	3D reality [mm]	PAT images [mm]	Final 2D images [mm]
Phantom 1	5	30.6 ± 0.5	32 ± 1.8	29 ± 0.5
	5	20.2 ± 0.6	21.4 ± 0.97	21.8 ± 1.6
Phantom 2	6	29.8 ± 0.5	28.7 ± 1.5	29.5 ± 1.4

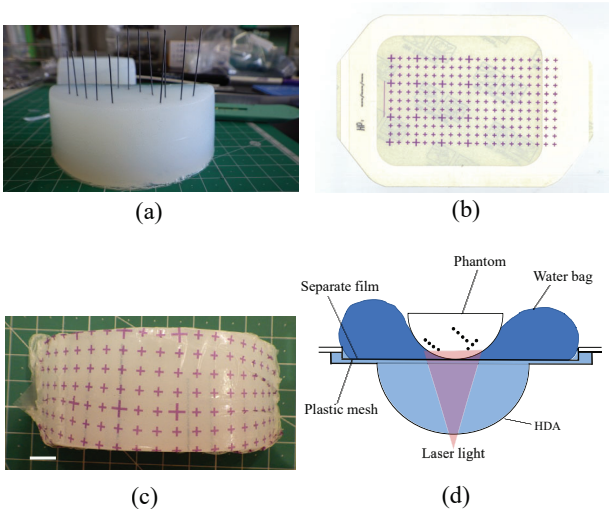

Fig. 6. Phantom preparation. (a) After completely cooling down the 5% agarose gel, HB 0.5 mm leads were inserted by pushing them into the gel. (b) Violet crosses were printed using a ultraviolet printer on Tegaderm film, (c) which was applied on the phantom just before the PAT experiment. (d) Schematic of the PAT imaging configuration. White scale bar represents 1 cm.

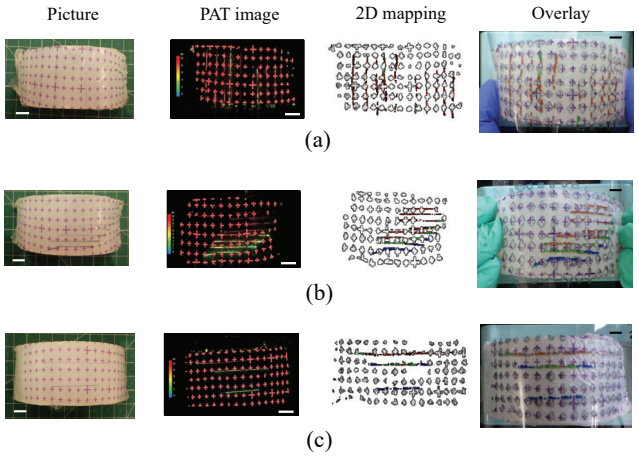

Fig. 7. Pictures, PAT images, 2D mapping images, and overlay of the final printed sheets of (a) Phantom 1, (b) Phantom 2, and (c) Phantom 3. In the PAT images reconstructed after analysis, the crosses were in red because they were selected to demonstrate the proposed method of analysis using the PAT viewer. The color scale bar indicates the distance between the point and the surface, represented by the violet crosses. The colors in the reconstructed 2D mapping images refer to the depth scale defined by the PAT viewer. White scare bar represents 1 cm. Black scale bar represents 0.5 cm.

value is arch length. The results in Table II clearly show a good match between data from the 2D images and theoretical calculations based on the geometry of the phantom.

B. Clinical Experiment

Clinical experiments were conducted to verify if PreFlap is useful for controlling the morphology of selected vessels in 3D and improving the understanding of the perfusion territory. Two different types of flaps were selected to prove the validity of the method: an ALT flap (Fig. 3(a)) and a transverse abdominal flap with a deep inferior epigastric perforator (DIEP flap) (Fig. 3(b)). In a DIEP flap, only skin and fat are removed from the abdomen to form a new breast mound [12]. In the ALT flap, skin is taken from the thigh and can be used to fill a hole left when a cancer has been removed in the head and neck [20]. The clinical results were verified and validated using US images and ICG angiography.

This study was approved by the ethics committee of the Kyoto University Graduate School of Medicine (protocol number: Y0083, approval date : on Feb. 8th, 2021) and was conducted in accordance with the Declaration of Helsinki. Written informed consent was obtained from all patients. Name of the clinical trial: "A Clinical Trial of Diagnostic Photoacoustic Imaging System in the Planning of Free Flap Surgery". Clinical trial number: jRCTs052200139. Webpage: https://jrct.niph.go.jp/en-latest-detail/jRCTs052200139.

TABLE II
LEAD LENGTH MEASUREMENT RESULTS FOR PHANTOM 3

Lead	Property	3D reality [mm]	PAT images [mm]	Final 2D images [mm]
Lead 1	Chord C	30	21.2	–
	Sagitta S	3	3	–
	Arch A	30	26.5	25
Lead 2	Chord C	37	34.9	–
	Sagitta S	5	5.5	–
	Arch A	39	38.4	40
Lead 3	Chord C	60	50.9	–
	Sagitta S	14	13.8	–
	Arch A	67	59.5	64

It was not possible to evaluate the radius and angle due to the field of view limit of 30 mm, for the phantom thickness (8(a)). In addition, in the final 2D images, only arch length (A) was evaluable (8(c)).

The clinical protocol's workflow consists of three steps. First, 3D PAT image acquisition on the interest area was performed. The surgeon drew references on the skin and used US to localize the perforators.Second, PAT viewer analysis was used to select the perforators as well as artery and vein patterns and create three output files as described in Section II-B.2). Third, 3D images were converted into 2D images.

1) Preoperative patient images: PAT imaging was performed 5 to 7 days before surgery. US was performed using a HI VISION Ascendus US machine (Hitachi, Tokyo, Japan). The perforators predicted with US were marked on patient's skin in red ink, which is not detectable by PAT. A 2 cm × 2 cm grid of crosses (12 cm × 8 cm in area) was marked with purple ink, which is detectable with PAT at 756 nm. A scan of a 12 cm × 6 cm region in high-resolution mode took approximately 18 minutes (Fig. 9(b) and Fig. 10(b)). The red and purple marks on each patients' skin were preserved by covering the skin with sheets of transparent medical film until the day of surgery. The veins and arteries were tracked with the PAT viewer to create networks of hypothesized arteries and hypothesized veins. Subsequently, these 3D data were computed to create 2D images and printed onto projector film sheets (A-one, 3M) using a VersaUV LeF-12i ultraviolet printer (Roland DG Co.). These transparent vascular maps were completed before the day of surgery, laminated with Vega4 (Fellowes, Itasca, IL 60143, USA), and sterilized with STERRAD (Johnson & Johnson, New Brunswick, New Jersey,USA) to bring them into

This article has been accepted for publication in IEEE Transactions on Biomedical Engineering. This is the author's version which has not been fully edited and content may change prior to final publication. Citation information: DOI 10.1109/TBME.2023.3293812

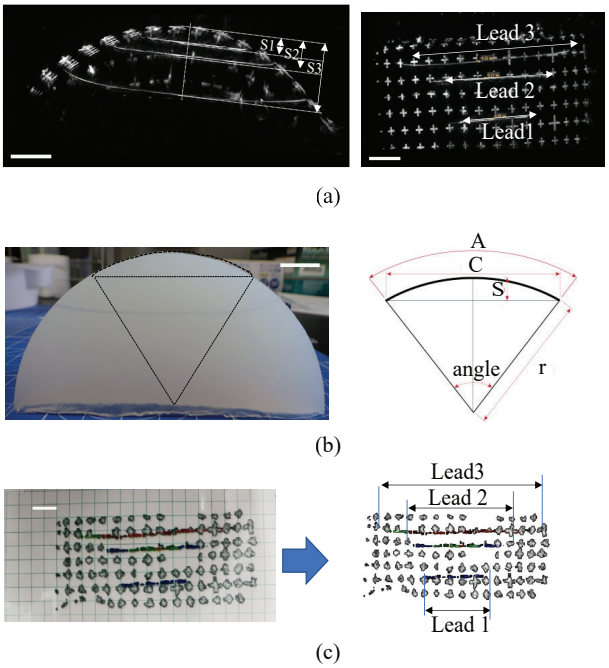

Fig. 8. Results of analysis on phantom 3. (a) Values defined based on Photoacoustic tomography (PAT) images. (b) Values defined from images using ImageJ Fiji. Dotted lines are representative lines used in the validation. Values are indicated in the schematic. (c) Values from two-dimensional (2D) printed images measured with a ruler. White scale bar represents 1 cm.

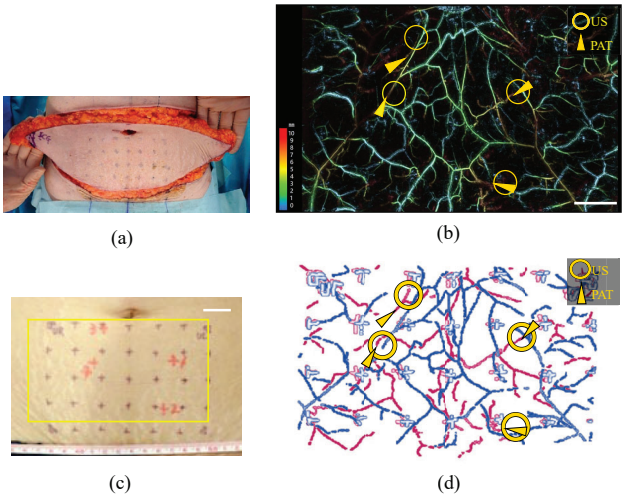

Fig. 9. (a) Deep inferior epigastric perforator (DIEP flap). (b) High-resolution PAT image representing depth. (c) Image of the body with the high-resolution mapping area indicated by the yellow rectangle. (d) Overlap of the 2D vascular maps. Hypothesized veins are indicated in blue. Hypothesized arteries are indicated in magenta. Abbreviations used in the figure: Photoacoustic tomography (PAT), Doppler ultrasonography (US). White scale bar represents 2 cm.

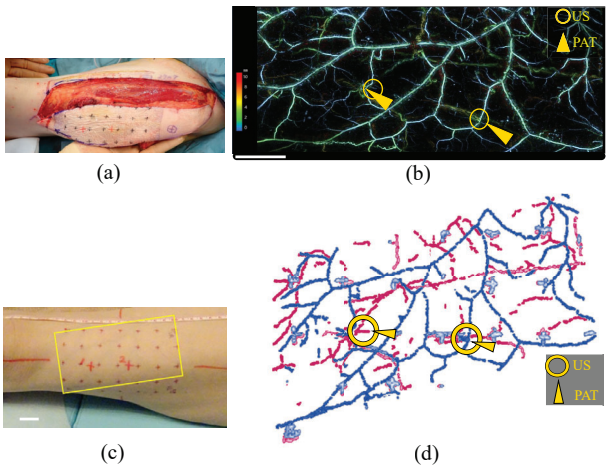

Fig. 10. (a) Anterolateral thigh (ALT) flap. (b) High-resolution PAT image representing depth. (c) Image of the body with the high-resolution mapping area indicated by the yellow rectangle. (d) Overlap of the 2D vascular maps. Hypothesized veins are indicated in blue. Hypothesized arteries are indicated in magenta. Abbreviations used in the figure: Photoacoustic tomography (PAT), Doppler ultrasonography (US).White scale bar represents 2 cm.

the surgical field.

2) Intraoperative ICG test and validation method: On the day of surgery, the skin surface was disinfected with povidone-iodine. The reference points were re-marked and a new film of Tegaderm was applied to preserve the reference crosses during surgery. After flap elevation, the area around the flap was covered by a blue drape and 2 mL of ICG (2.5 mg/mL; Diagnogreen; Daiichi Sankyo Co., Tokyo, Japan) was injected intravenously. ICG is a water-soluble fluorescent dye with a spectral absorption range and peak emission of 750–800 nm and 832 nm, respectively. Once injected, visualization of dye distribution was performed with an 806 nm near infrared (NIR) laser with a penetration depth of up to 2 cm, which corresponds to the level of the fascia [6], [31]. The ICG emission signals were detected with PDE-neo (Hamamatsu Photonics Inc., Shizuoka, Japan). ICG image recording in real time started immediately after injection of the dye and lasted for approximately 2–3 minutes. The arterial phase was defined as the stage in which fluorescence imaging begins and spreads for approximately 20–30 seconds after injection. The venous phase was defined as the stage when ICG is visible in the flap after approximately 50–90 seconds [32].

Manual characterization of ICG videos was performed in ImageJ Fiji [33]. The video processing workflow involved three steps (Fig. 11). In the first step, crosses were added as an annotation on the violet reference crosses on the skin (collected in color mode on the recorded ICG video) and the file was saved in the selection format. Images at three different time points were saved in JPG format: (1) at the start (color mode), (2) arterial phase, and (3) venous phase. In the second step, these images were analyzed. The ICG images are not clearly delineated due to the weak signal from slow blood flow or deeper vessels. Therefore, the Frangi filter was applied. This filter is commonly used in the analysis of angiography images since it reduces the impact of intensity variations along a vessel and suppresses background noise, thereby improving image segmentation [34]. The binarized image (vessel or non-vessel) was skeletonized by ImageJ Fiji and a mask was created. In the last step, the selection with annotations was applied to the masks and saved as JPG.

This article has been accepted for publication in IEEE Transactions on Biomedical Engineering. This is the author's version which has not been fully edited and content may change prior to final publication. Citation information: DOI 10.1109/TBME.2023.3293812

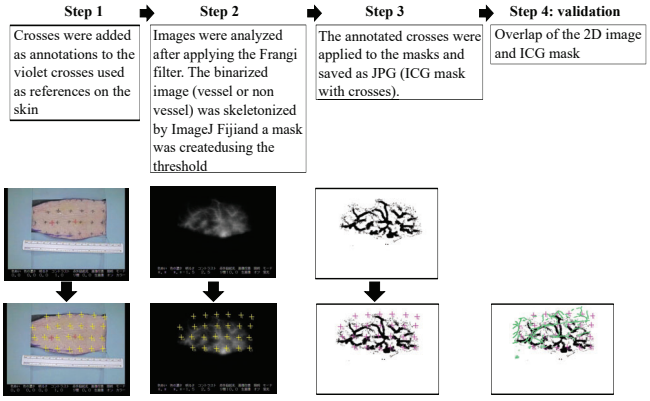

Fig. 11. Method for ICG image analyses, and exemplar images.

3) Clinical Experiment Results: Merged images of the hypothesized arterial and venous patterns (printed transparent vascular maps) and the arterial and venous phases (mask images by ImageJ Fiji) were created by overlaying the violet crosses (references on the patient's skin, which were visible on the PAT images), and the crosses annotated on the ICG video. Similarly, the vascular maps printed on transparent material were placed over the patient's skin during the surgery.

The results for two flaps are shown in Fig. 9 and Fig. 10. The 2D images of selected arteries and veins were compared with the original PAT data. Perforators identified with PAT were confirmed using US. The ICG arterial and venous phases were analyzed and compared with the 2D vascular maps as shown in Fig. 12 and Fig. 13. The overlap of the 2D images and ICG shows that the unwrapping procedure for the 2D vascular maps worked well and that these printed images can be used as guides or references by the surgeon. The images reveal an imperfect match of the crosses on the skin and the 2D printed maps. This is the consequence of differences in skin shrinkage along different directions after flap elevation (Fig. 14). The match rate was calculated as the percentage of vessels in ICG images that match with vessels on 2D mapping sheets. Users manually outlined the vessels as multiple regions of interest (ROIs) using ImageJ, added to the ROI manager, and then measured them. In the arterial phase, the match rate was 69.5% and 63.4%, for DIEP and ALT flaps respectively. In the venous phase, the match rate was 75.5% and 78.2%, for DIEP and ALT, respectively.

IV. Discussion

The ability to design and transfer flaps to repair tissue defects is a fundamental skill in reconstructive surgery. The success of a perforator flap depends on the integrity of the perforator vessel. However, since the exact position of the perforator varies and can never be predicted precisely based on clinical experience, the objective of preoperative planning is defining the flap vascular architecture to facilitate perforator dissection and speed up flap elevation (Figs. 1(a)).

PAT can create 3D images of blood vessel patterns with an in-depth resolution of about 3 cm. This technology provides images of small-caliber blood vessels to examine vascular

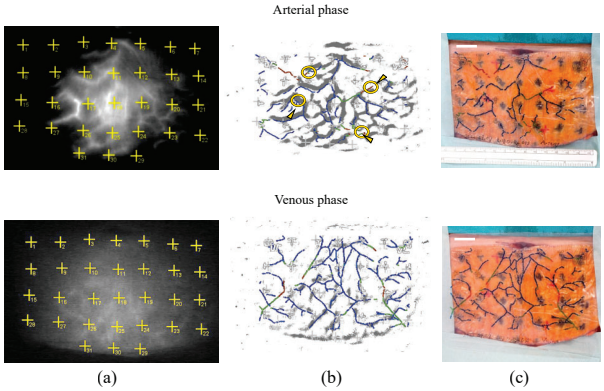

Fig. 12. Deep inferior epigastric perforator (DIEP) flap: (a) ICG image during arterial and venous phases. Brightness and contrast adjustments have been made to make the ICG images clearer. (b) 2D vascular mapping over ICG mapping (black and white) . (c) Overlap of 2D printed images and the DIEP flap after flap elevation. White scale bar represents 2 cm.

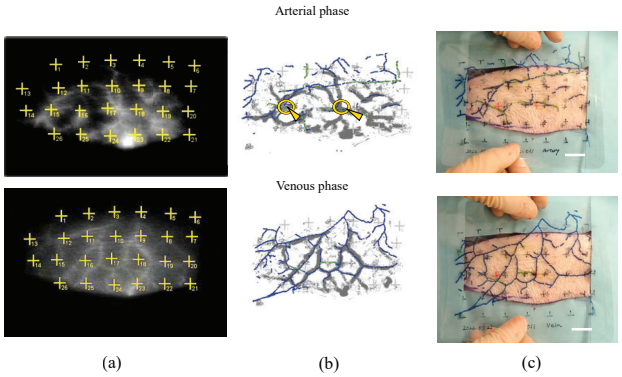

Fig. 13. Anterolateral thigh (ALT) flap :(a) ICG image during arterial and venous phases.Brightness and contrast adjustments have been made to make the ICG images clearer. (b) 2D vascular mapping over ICG mapping (black and white). (c) Overlap of 2D printed images and the ALT flap after flap elevation. White scale bar represents 2 cm.

connections. Thus, it is the ideal system to create detailed images of flap regions to study and to localize perforators and the perfusion territory. However, the 3D maps can be difficult to conceptualize. Complementary technologies are necessary for preoperative planning and during the procedure. Indeed, a technology with augmented reality environments that adjust for skin deformation would be the best method, but creating a realistic 3D skin deformation model that can be used intraoperatively remains challenging. Thus, we have focused our research on creating 2D vascular maps that can highlight anatomical variations and can assist the surgeon in choosing the appropriate perforator and perfusion territory.

The PreFlap software program, which uses PAT imaging to create 2D vascular mapping images of the 3D blood vessel network, was developed. We demonstrated its ability to create unwrapped surfaces that match the 3D object's real shape using curved phantoms. We were able to compare the 3D object's points with points in the unwrapped image to evaluate the accuracy of the unwrapping procedure. We verified the validity of the approximation parameter c, which was defined

This article has been accepted for publication in IEEE Transactions on Biomedical Engineering. This is the author's version which has not been fully edited and content may change prior to final publication. Citation information: DOI 10.1109/TBME.2023.3293812

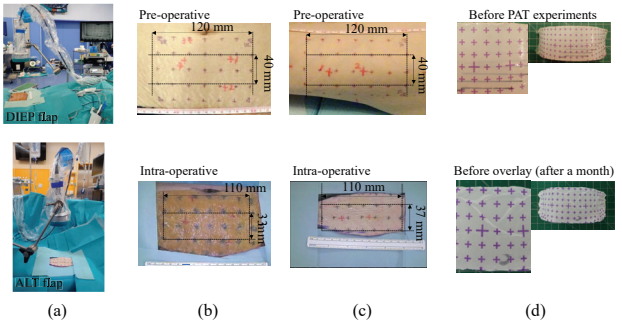

Fig. 14. (a) Configuration for indocyanine green (ICG) data acquisition in the operating room. Stretching of the skin in the (b) deep inferior epigastric perforator (DIEP) ICG and (c) anterolateral thigh (ALT) flaps. (d) Movement of the Tegaderm film on the phantom. The difference in color of the phantom is due to the different lighting conditions in the operating room.

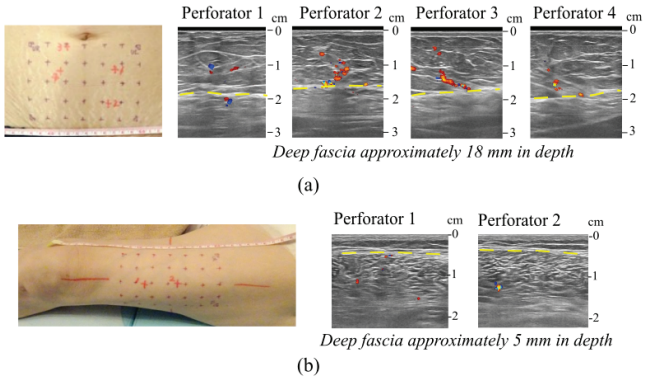

Fig. 15. Ultrasonography of (a) deep epigastric perforators, and (b) anterolateral thigh flaps.

to calculate the approximated arc length (Fig. 3(c)). The goal was to unwrap each image so that all objects in the image are co-planar (2D) and do have any distortions. We showed that PreFlap creates a single unwrapped planar image of 3D objects such as cross references and thin and straight objects (leads) located at any distance distances from the Tegaderm film (surface representing the location nearest to the PAT detectors) up to 30 mm deep (field of view).

In clinical studies, we assessed the potential benefits of the 2D vascular maps of flap regions. Two different types of flaps were selected to demonstrate the validity of the method: DIEP and ALT flaps. These types of flaps were selected because they represent situations with different critical control points. In an abdominal flap, a very large area of skin is used. Therefore, understanding of the perfusion region is crucial for a positive surgical outcome. The flap is almost flat, so deformations due to the rectification and unwrapping of the skin are not expected. Instead, in the thigh flap, the flap region is small, but there is more curvature of the skin. Thus, differences or deformations due to the flap's condition before and during surgery might strongly affect the localization of perforators and main branches. The overlap between the printed sheets and body skin showed an imperfect match of the references; however, these differences were smaller than 2–5 mm, and thus considered negligible. In fact, it is well known that the skin has direction-dependent biomechanical behavior. Therefore, after flap elevation, skin contraction is unevenly distributed. The contraction rate of skin varies according to anatomical region and follows skin tension lines [34], [35]. As a consequence of skin contraction, it is difficult for the surgeon to extend the skin to its original configuration (Fig. 14). Thus, it is impossible to obtain a perfect match of the crosses.

Fig. 1(b) is a schematic representation of the presented method. The surgeon draws violet crosses (references) on the patient's skin. With US analysis, the surgeon can draw the location where the perforator exits the fascia with a red pen. US was performed to validate PAT results in our experiments. These red lines cannot be visualized in PAT images. Instead violet lines can be visualized in the image collected at 756 nm. Since PAT images are collected at 756 and 797 nm, it is possible to analyze the arterial and venous subcutaneous networks separately [23], and perforators can be identified with measurement errors smaller than 5 mm. These features improve the safety of the surgical procedure which can be performed smoothly and more quickly. The results of the 2D mapping were verified using ICG. ICG provides the final confirmation of the perfusion area during flap surgery. The time delay from ICG administration to the first significant increase in fluorescence intensity is variable; it is affected by the thickness of skin and subcutaneous fat. The delay can be in the range of a few tens of seconds. Next, fluorescence intensity in the arteries continues to increase until the maximum intensity is reached. This interval is defined the arterial phase (or arterial inflow). Subsequently, ICG passes into the veins and reaches a maximum intensity; this second interval is defined as the venous phase or venous outflow. Next, ICG fluorescence intensity reaches a plateau (plateau phase) before it is slowly eliminated. The plateau phase is characterized by diffuse fluorescence showing the area of perfusion and dark areas correlated with poor perfusion. For example, in DIEP flaps, when the flap has good circulation, the fluorescence showed homogeneous and usually only zone IV has very weak or no fluorescence, which indicates poor perfusion (Fig. 3) [36]. In this study we used the difference in ICG transit time between arterial inflow and venous outflow [32] to visualize arterial and venous patterns separately. Thus, two images were obtained from the analysis of the ICG videos and compared to the 2D vascular maps (Fig. 12 and Fig. 13). Systemic perfusion factors are likely to affect local fluorescence intensity [36], [37]. Therefore, it is not surprising that the venous phase is clearly observable in ALT flaps and less clear in DIEP flaps. The ICG images collected in DIEP flaps were clearer and the match rate was higher in the arterial phase (69.5% and 63.4%, for DIEP and ALT flaps, respectively). Instead, in the venous phase, the images collected in the DIEP flaps were less clear than the images for ALT flaps. The match rates were 75.5% and 78.2%, for DIEP and ALT flaps, respectively. It is important to note that some non-overlapping vessels on the 2D mapping sheets appeared as deeper vessels (green and red colors indicate a depth deeper than 4–7 mm (Fig. 12 and Fig. 13)). Several studies have shown that ICG skin penetration

depth is approximately 1 cm [38], [39]. However, other studies have reported that ICG can be detected up to 2 cm [6], [31]. Thus, we suggest that this difference in how the vessels are visualized, which affects the match rate, might be related to ICG depth resolution.

In PAT images, as well as in the 2D mapping sheets, perforators were identified as deeper vessels (red-green branches (Fig. 12 and Fig. 13)) with an appropriate external diameter that give off two or three small branches that are running up to the skin (blue branches). The perfusion area is then defined following the course of the branches diverging from this vessel up to the skin. The overall accuracy of the prediction was confirmed by both the US and ICG results. From the 2D images of artery and vein patterns, surgeons can predict the location of perforators and branches, with errors smaller than 2–5 mm. This aids surgeons in selecting the best perforator(s) to optimize flow and perfusion within a flap in order to minimize the incidence of fat or partial flap necrosis. In fact, it is difficult to detect discrepancies between the perforating arteries and veins using US or CTA. And other mapping methods such as ICG mapping can only be used intraoperatively. Thus, the combined use of 3D PAT mapping and 2D vascular maps makes it possible to identify the number and location of perforators within the area designed to be part of a flap, which can enhance the surgeon's confidence during surgery and make the procedure easier, faster, and more reliable.

While interpreting these data, it is important to recognize that matching the crosses on the skin and on the 2D sheet is necessary to use as validation method the ICG mapping. Our suggested method enables the surgeon mentally to resize the location of the perforator(s) and branches according to the aid of the 2D mapping sheet when the skin contracts after flap elevation, as well. In fact, without a 3D model that can automatically adjust the vascular map according to the skin contraction, 3D images become difficult to conceptualize after flap elevation. Instead, 2D mapping sheets with detailed information on the subcutaneous vessels enables surgeons to design complex flaps more easily without reducing the blood supply. Indeed, these 2D mapping sheets can be used on elevated flaps. Since they are made with transparent plastic sheets, they can be used also when the flap is turned upside down.

In this work, we take an important step forward in making PAT clinically feasible. Although it would be interesting to use artificial intelligence for automated detection of dominant perforators, the mapping sheets are now semi-automatically prepared. They provide accurate information more quickly than in the previous study of Tsuge et al [20]. However, it would be useful to prepare a virtual model based on an imaging modality and display it on top of the patient's skin. It might be able to adjust the projected images to the skin local deformations after flap elevation using corrective software.

V. Conclusion

Preoperative evaluation of perforator flaps and the perfusion area is possible with a PAT imaging system [18]–[21]. In this study, we have demonstrated that PreFlap can convert 3D PAT images into 2D vascular maps where perforating vessels and branches are clearly indicated to support the surgeon in visualizing the undersurface of the flap. Therefore, PreFlap is a useful tool for visualizing hypothetical arterial and venous networks and designing the perfusion territory during preoperative surgery planning.

Acknowledgment

We would like to express our sincere gratitude to all our collaborators: Ayako Takaya, Minako Chaya, Aya Yoshikawa, Hiroyuki Sekiguchi, Kenichi Nagae, Osamu Arai, Takeshi Suwa, Yasufumi Asao, and Takayuki Yagi.

Data Availability

The data and computer code are not publicly available due to commercial and patent restrictions.

Author Disclosure Statements

The authors declare no competing interests.

References

[1] L. Qing, P. Wu, Z. Bing, F. Yu, X. Pang, P. Ding, Z. Lei, Y. Xiao, J. Fu, and J. Tang, "The concept of the special form perforator flap and its role in the evolution of reconstruction," *Journal of Xiangya Medicine*, vol. 4, feb 2019.

[2] J. T. Kim and S. W. Kim, "Perforator flap versus conventional flap," pp. 514–522, 2015.

[3] G. Tenekeci, "Perforator Flaps: Principles and Techniques," in *Issues in Flap Surgery*. InTech, apr 2018.

[4] T. Yamamoto, N. Yamamoto, T. Kageyama, H. Sakai, Y. Fuse, K. Tsuihiji, and R. Tsukuura, "Definition of perforator flap: what does a "perforator" perforate?" *Global Health & Medicine*, vol. 1, no. 2, pp. 114–116, dec 2019.

[5] J. Wade, Ryckie G.and Watford, J. C. Wormald, R. J. Bramhall, and A. Figus, "Perforator mapping reduces the operative time of DIEP flap breast reconstruction: A systematic review and meta-analysis of preoperative ultrasound, computed tomography and magnetic resonance angiography," *Journal of Plastic, Reconstructive and Aesthetic Surgery*, vol. 71, no. 4, pp. 468–477, April 2018.

[6] Y. M. Khoong, X. Huang, S. Gu, and T. Zan, "Imaging for thinned perforator flap harvest: current status and future perspectives," *Burns & Trauma*, vol. 9, January 2021.

[7] B. Versluis, S. Tuinder, C. Boetes, R. Van Der Hulst, A. Lataster, T. Van Mulken, J. Wildberger, M. de Haan, and T. Leiner, "Equilibrium-phase high spatial resolution contrast-enhanced mr angiography at 1.5t in preoperative imaging for perforator flap breast reconstruction," *PLOS ONE*, vol. 8, no. 8, pp. 1–7, 08 2013. [Online]. Available: https://doi.org/10.1371/journal.pone.0071286

[8] A. Cina, M. Salgarello, L. Barone-Adesi, P. Rinaldi, and L. Bonomo, "Planning breast reconstruction with deep inferior epigastric artery perforating vessels: Multidetector CT angiography versus color Doppler US," *Radiology*, vol. 255, no. 3, pp. 979–987, jun 2010.

[9] J. González Martínez, A. Torres Pérez, M. Gijón Vega, and T. Nuñez-Villaveiran, "Preoperative Vascular Planning of Free Flaps: Comparative Study of Computed Tomographic Angiography, Color Doppler Ultrasonography, and Hand-Held Doppler," *Plastic and Reconstructive Surgery*, vol. 146, no. 2, pp. 227–237, aug 2020.

[10] M. Y. Nahabedian and K. M. Patel, "Maximizing the Use of the Handheld Doppler in Autologous Breast Reconstruction," pp. 213–218, apr 2011.

[11] J. M. Smit, S. Klein, and P. M. Werker, "An overview of methods for vascular mapping in the planning of free flaps," sep 2010.

[12] A. Alonso-Burgos, E. García-Tutor, G. Bastarrika, D. Cano, A. Martínez-Cuesta, and L. J. Pina, "Preoperative planning of deep inferior epigastric artery perforator flap reconstruction with multislice-CT angiography: imaging findings and initial experience," *Journal of Plastic, Reconstructive and Aesthetic Surgery*, vol. 59, no. 6, pp. 585–593, jun 2006.

[13] L. Jung Woo, K. Han Kyeol, Kimand Sin Rak, H. Yea Sik, and P. Jin Hyung, "Preoperative Identification of a Perforator Using Computed Tomography Angiography and Metal Clip Marking in Perforator Flap Reconstruction," *Archives of Plastic Surgery*, vol. 42, no. 1, pp. 78–83, jan 2015.

[14] S. H. Bailey, M. Saint-Cyr, C. Wong, A. ojallal, K. Zhang, D. Ouyang, G. Arbique, A. Trussler, and R. R. J., "The Single Dominant Medial Row Perforator DIEP Flap in Breast Reconstruction: Three-Dimensional Perforasome and Clinical Results," *Plastic and Reconstructive Surgery*, vol. 126, no. 3, pp. 739–751, Sept 2010.

[15] C. Wong, M. Saint-Cyr, A. Mojallal, T. Schaub, S. H. Bailey, S. Myers, S. Brown, and R. J. Rohrich, "Perforasomes of the DIEP flap: vascular anatomy of the lateral versus medial row perforators and clinical implications," *Plastic and Reconstructive Surgery*, vol. 125, no. 3, pp. 772–782, Mar 2010.

[16] Y. Shen, J. Huang, M.-J. Dong, J. Li, W.-M. Ye, and J. Sun, "Application of Computed Tomography Angiography Mapping and Located Template for Accurate Location of Perforator in Head and Neck Reconstruction with Anterolateral Thigh Perforator Flap," *Plastic and Reconstructive Surgery*, vol. 137, no. 6, pp. 1875–1885, Jun 2016.

[17] S. Hummelink, Y. L. Hoogeveen, L. J. Schultze Kool, and D. J. O. Ulrich, "A New and Innovative Method of Preoperatively Planning and Projecting Vascular Anatomy in DIEP Flap Breast Reconstruction: A Randomized Controlled Trial," *Plastic and Reconstructive Surgery*, vol. 143, no. 6, pp. 1151e–1158e, June 2019.

[18] S. Saito, R. Bise, A. Yoshikawa, H. Sekiguchi, I. Tsuge, and M. Toi, "Digital artery deformation on movement of the proximal interphalangeal joint," *Journal of Hand Surgery: European Volume*, vol. 44, no. 2, pp. 187–195, feb 2019.

[19] I. Tsuge, S. Saito, H. Sekiguchi, A. Yoshikawa, Y. Matsumoto, M. Toi, and S. Suzuki, "Photoacoustic Tomography Shows the Branching Pattern of Anterolateral Thigh Perforators in Vivo," *Plastic and Reconstructive Surgery*, vol. 141, no. 5, pp. 1288–1292, may 2018.

[20] I. Tsuge, S. Saito, G. Yamamoto, H. Sekiguchi, A. Yoshikawa, Y. Matsumoto, S. Suzuki, and M. Toi, "Preoperative vascular mapping for anterolateral thigh flap surgeries: A clinical trial of photoacoustic tomography imaging," *Microsurgery*, vol. 40, no. 3, pp. 324–330, mar 2020.

[21] H. Shimizu, S. Saito, A. Yoshikawa, H. Sekiguchi, I. Tsuge, N. Morimoto, and M. Toi, "Three-dimensional Visualization of Thoracodorsal Artery Perforators Using Photoacoustic Imaging," *Journal of Plastic, Reconstructive & Aesthetic Surgery*, jun 2022.

[22] Y. Asao, K. Nagae, K. Miyasaka, H. Sekiguchi, S. Aiso, S. Watanabe, M. Sato, S. Kizaka-Kondoh, Y. Nakajima, K. Kishi, and T. Yagi, "In Vivo Label-Free Observation of Tumor-Related Blood Vessels in Small Animals Using a Newly Designed Photoacoustic 3D Imaging System," *Ultrasonic Imaging*, vol. 44, no. 2-3, pp. 96–104, may 2022.

[23] Y. Matsumoto, Y. Asao, A. Yoshikawa, H. Sekiguchi, M. Takada, M. Furu, S. Saito, M. Kataoka, H. Abe, T. Yagi, K. Togashi, and M. Toi, "Label-free photoacoustic imaging of human palmar vessels: A structural morphological analysis," *Scientific Reports*, vol. 8, no. 1, dec 2018.

[24] Y. Matsumoto, Y. Asao, H. Sekiguchi, A. Yoshikawa, T. Ishii, K. ichi Nagae, S. Kobayashi, I. Tsuge, S. Saito, M. Takada, Y. Ishida, M. Kataoka, T. Sakurai, T. Yagi, K. Kabashima, S. Suzuki, K. Togashi, T. Shiina, and M. Toi, "Visualising peripheral arterioles and venules through high-resolution and large-area photoacoustic imaging," *Scientific Reports*, vol. 8, no. 1, dec 2018.

[25] I. Yamaga, N. Kawaguchi-Sakita, Y. Asao, Y. Matsumoto, A. Yoshikawa, T. Fukui, M. Takada, M. Kataoka, M. Kawashima, E. Fakhrejahani, S. Kanao, Y. Nakayama, M. Tokiwa, M. Torii, T. Yagi, T. Sakurai, H. Haga, K. Togashi, T. Shiina, and M. Toi, "Vascular branching point counts using photoacoustic imaging in the superficial layer of the breast: A potential biomarker for breast cancer," *Photoacoustics*, vol. 11, pp. 6–13, sep 2018.

[26] H. Sekiguchi, A. Yoshikawa, Y. Matsumoto, Y. Asao, T. Yagi, K. Togashi, and M. Toi, "Development of the rapid MIP viewer for PAT data—KURUMI: Kyoto University rapid and universal MIP imager." *IEICE Tech Report. Medical Imaging*, pp. 163–167, 2017.

[27] J. Palma-Chavez, K. A. Wear, Y. Mantri, J. V. Jokerst, and W. C. Vogt, "Photoacoustic imaging phantoms for assessment of object detectability and boundary buildup artifacts," *Photoacoustics*, vol. 26, jun 2022.

[28] F. Vasefi, R. Saager, A. J. Durkin, N. MacKinnon, E. Gussakovsky, R. Chave, and D. L. Farkas, "Quantifying the optical properties and chromophore concentrations of turbid media using polarization sensitive hyperspectral imaging: optical phantom studies," in *Imaging, Manipulation, and Analysis of Biomolecules, Cells, and Tissues XI*, vol. 8587. SPIE, feb 2013, p. 85870Z.

[29] E. Maneas, W. Xia, O. Ogunlade, M. Fonseca, D. I. Nikitichev, A. L. David, S. J. West, S. Ourselin, J. C. Hebden, T. Vercauteren, and A. E. Desjardins, "Gel wax-based tissue-mimicking phantoms for multispectral photoacoustic imaging," *Biomedical Optics Express*, vol. 9, no. 3, p. 1151, mar 2018.

[30] T. Weller, "Multi-Layer RF Tissue Phantoms for Mimicking a Human Core Quenton Bonds," in *2017 IEEE International Conference on Microwaves, Antennas, Communications and Electronic Systems (COMCAS)*, 2017, pp. 1–4. [Online]. Available: doi: 10.1109/COMCAS.2017.8244763

[31] H. Sheriff, C. Vega Garcia, J. Garcia Lorenzo, S. Lopez Fernandez, S. S. Kareem, C. Hankins, J. Masia, and M. Fernandez Garrido, " Indocyanine Green Angiography in Salvage Planning: From Pedicled Supraclavicular Flap to Free Supraclavicular Flap. ," *International Microsurgery Journal*, vol. 5, no. 1, p. 4, Sep 2021.

[32] K. Li, Z. Zhang, F. Nicoli, C. D'Ambrosia, W. Xi, D. Lazzeri, S. Feng, W. Su, H. Li, P. Ciudad, M. Tremp, and Y. X. Zhang, "Application of Indocyanine Green in Flap Surgery: A Systematic Review," pp. 77–86, feb 2018.

[33] J. Schindelin, I. Arganda-Carrera, E. Frise, K. Verena, L. Mark, P. Tobias, P. Stephan, R. Curtis, S. Stephan, S. Benjamin, T. Jean-Yves, J. W. Daniel, H. Volker, E. Kevin, T. Pavel, and C. Albert, "Fiji - an Open platform for biological image analysis," *Nature Methods*, vol. 9, no. 7, 2009.

[34] A. F. Frangi, W. J. Niessen, K. L. Vincken, and M. A. Viergever, "Multiscale vessel enhancement filtering," in *Medical Image Computing and Computer-Assisted Intervention — MICCAI'98*, W. M. Wells, A. Colchester, and S. Delp, Eds. Berlin, Heidelberg: Springer Berlin Heidelberg, 1998, pp. 130–137.

[35] S. J. Salasche and W. J. Crabski, "Complications of Flaps," *J Dermatol Surg Oncol*, vol. 17, pp. 132–140, 1991.

[36] N. Girard, M. Delomenie, C. Malhaire, D. Sebbag, A. Roulot, A. Sabaila, B. Couturaud, J.-G. Feron, and F. Reyal, "Innovative DIEP flap perfusion evaluation tool: Qualitative and quantitative analysis of indocyanine green-based fluorescence angiography with the SPY-Q proprietary software," *PLOS ONE*, vol. 14, no. 6, p. e0217698, June 2019.

[37] T. Desmettre, J. M. Devoisselle, and S. Mordon, "Fluorescence Properties and Metabolic Features of Indocyanine Green (ICG) as Related to Angiography," *Survey of Ophthalmology*, vol. 45, no. 1, pp. 15–27, July 2020.

[38] J.-H. Kim, M. Ku, J. Yang, and H. K. Byeon, " Recent Developments of ICG-Guided Sentinel Lymph Node Mapping in Oral Cancer." *Diagnostics*, vol. 11, no. 5, p. 891, May 2021.

[39] M. Griffiths, M. P. Chae, and W. M. Rozen, " Indocyanine green-based fluorescent angiography in breast reconstruction. ," *Gland surgery*, vol. 5, no. 5, pp. 133–149, April 2016.